Stochastic Environmental Research and Risk Assessment (2021) 35:1529–1547
https://doi.org/10.1007/s00477-021-02006-z

ORIGINAL PAPER

Upscaling bimolecular reactive transport in highly heterogeneous porous media with the LAgrangian Transport Eulerian Reaction Spatial (LATERS) Markov model

Elise E. Wright[1] · Nicole L. Sund[2] · David H. Richter[1] · Giovanni M. Porta[3] · Diogo Bolster[1]

Accepted: 18 March 2021 / Published online: 28 April 2021

Abstract
The LAgrangian Transport Eulerian Reaction Spatial (LATERS) Markov model was developed to predict upscaled bimolecular reactive transport in a flow around an array of solid cylinders. This method combines the stochastic Lagrangian Spatial Markov model (SMM) to predict transport and a volume averaged reaction rate equation to predict reactions of the form $A + B \rightarrow \emptyset$. Here, we extend the LATERS Markov model to upscale bimolecular reactive transport in a Darcy flow through an idealized heterogeneous porous medium. In agreement with previous literature, the accuracy of the prediction is a function of the Damköhler (Da) numbers, i.e., high Da are more challenging because of incomplete mixing. It was found that a key component which must be incorporated into the upscaled model in these high Da systems is the idea that nearby A and B particles should be more likely to react than those that are farther apart. This is here achieved by appropriately reducing the resolution of the spatial grid employed to resolve the reactive process.

Keywords Reactions · Markov model · Heterogeneous

1 Introduction

Flows in the subsurface are complex as they are characterized by heterogeneous geological structures across a broad range of scales Dentz et al. (2011). This heterogeneity has a strong impact on transport, mixing, and chemical reactions. In real systems, the structure of the porous medium is in general unknown and difficult to determine. Even if it were possible to have knowledge of the full porous media structure, it is not computationally feasible to model these systems at larger scales of interest while still incorporating all of the pore scale information Dentz et al. (2011). This presents the need for upscaled models that can account for these small scale processes in an effective manner. Accurate prediction of chemical reactions in subsurface flows is important, as it has practical applications in predicting the fate and transport of contaminants Steefel et al. (2005); Yeh and Tripathi (1989) and the remediation of contaminated groundwater Mayer et al. (2006), Knutson et al. (2007), Committee (2013).

To study reactive transport, reactions between two solutes A and B that react to form a product P will be considered. Reactions of this form $A + B \rightarrow P$ have been shown to be the foundation for more complex reactions Gillespie (2007). Since the focus of this study is on how the reactive solutes A and B mix and react with one another, for simplicity the product of their reaction can be neglected, i.e. $A + B \rightarrow \emptyset$. For a case where A and B are initially distributed uniformly across the domain, there is a well-known analytical solution for the reactant concentrations under perfect mixing given by $C_A(x,y,t) = C_B(x,y,t) = C_0/(1+kC_0t)$, which scales like t^{-1} at late times. In general, real systems are not perfectly well-mixed and incomplete mixing will reduce the amount of reaction that takes place. For a homogeneous system where mixing occurs only by

✉ Elise E. Wright
ewright4@alumni.nd.edu

[1] Department of Civil and Environmental Engineering and Earth Sciences, University of Notre Dame, Notre Dame, IN 46556, USA

[2] Division of Hydrologic Sciences, Desert Research Institute, Reno, NV 89512, USA

[3] Dipartimento Ingegneria Civile ed Ambientale, Politecnico di Milano, Piazza L. Da Vinci, 32, Milano I-20133, Italy

dispersion and A and B are initially well-mixed, this slowdown in reaction rates has been shown to scale like $t^{-d/4}$, where d is the number of spatial dimensions. This result has been found in theory Kang and Redner (1984), Ovchinnikov and Zeldovich (1978), Doug and Frank (1983), numerical simulations Kang and Redner (1984), Ovchinnikov and Zeldovich (1978), Doug and Frank (1983), and laboratory experiments Monson and Kopelman (2000), Monson and Kopelman (2004).

While the case with reactants A and B initially well-mixed has received a lot of attention (e.g. Kang and Redner 1984; Monson and Kopelman 2000, 2004; Ovchinnikov and Zeldovich 1978; Paster et al. 2014, 2015; Doug and Frank 1983; Wright et al. 2017), a setup with A and B initially separated by a sharp interface is of interest as it has many real world applications. In this system, a reaction can only occur within the interface as A and B mix by dispersion and advection in the heterogeneous flow. A well-known experiment examined this setup in a one-dimensional uniform chamber and observed that there was a significant reduction in the amount of reaction product relative to the expected values under perfect mixing Gramling et al. (2002). This observed deviation from the well-mixed solution was due to the effects of incomplete mixing and many studies have worked to model the results of this experiment Edery et al. (2009), Edery et al. (2010), Sanchez-Vila et al. (2010), Chiogna and Bellin (2013), Ding et al. (2013), Alhashmi et al. (2015), Ginn (2018). It is clear from these results that incomplete mixing must be taken into account in order to accurately model reactive transport.

Upscaling reactive transport requires accurately accounting for transport, mixing, and reactions. These processes are inextricably linked to one another, making proper upscaling challenging. A variety of upscaled models have been developed with the goal of capturing the effects of incomplete mixing (e.g. Sanchez-Vila et al. 2010; Chiogna and Bellin 2013; Porta et al. 2016; Ginn 2018; Benson et al. 2019) and a review of many of these methods can be found in Dentz et al. (2011). These models must account for subscale concentration fluctuations that limit reaction. Lagrangian particle tracking methods have been shown to naturally account for such fluctuations and are unencumbered by numerical dispersion Benson et al. (2017), Boso et al. (2013). However, Eulerian methods are generally more computationally efficient in modeling chemical reactions relative to Lagrangian reactive transport models as they eliminate the need to search for nearby particles available for reaction. In this work, we aim to extend an existing hybrid reactive transport model that combines the strengths of both Lagrangian and Eulerian methods.

The Lagrangian Spatial Markov model (SMM) has been widely used to upscale mean conservative transport in a variety of systems, including fractured media Kang et al. (2011), Kang et al. (2015), Kang et al. (2017), Kang et al. (2011), Kang et al. (2015), Kang et al. (2016), complex pore-scale systems Kang et al. (2014), de Anna et al. (2013), and highly heterogeneous porous media Le Borgne et al. (2008a), Le Borgne et al. (2008b). In upscaling bimolecular reactive transport, knowledge of only the mean transport is insufficient. Information about local concentrations must be incorporated as well. The SMM was recently extended to predict upscaled mixing by developing several methods to predict particle locations that can be used to generate concentration fields and quantify mixing Wright et al. (2019). When modeling bimolecular reactions between two solutes A and B, it is crucial to not only appropriately quantify mixing of the reactive solutes themselves, but to adequately describe how A and B mix relative to one another.

For considering reactions in addition to conservative transport, an upscaled Eulerian reactive transport model was developed by Porta et al. (2012). This method volume averaged the advection diffusion reaction equation (ADRE) and developed a closure to account for subscale fluctuations Porta et al. (2012). While this model was able to upscale reactive transport and account for incomplete mixing effects, the closure problem entails nonlocal integro-differential terms which complicate the numerical solution of the system and play an important role at pre-asymptotic times Porta et al. (2016). The LAgrangian Transport Eulerian Reaction Spatial (LATERS) Markov model was developed by Sund et al. (2017) to predict bimolecular reactive transport in a simple two-dimensional porous medium consisting of a periodic array of solid cylinders. This method combines the ability of the SMM to upscale transport with the volume averaged reaction rate equation of Porta et al. (2012). In this work, we will extend the LATERS Markov model to upscale reactive transport in flows through idealized heterogeneous porous media.

2 System setup

We consider reactive transport in a flow through an idealized, two-dimensional heterogeneous porous medium. The flow field is obtained by first generating a log-normal random permeability field $\kappa(x, y)$ with zero mean and a variance of $\sigma^2_{\ln\kappa} = 9$. The permeability field is generated on a grid with square grid cells of unit area and has a selected correlation length $\lambda = 2$. The variance was chosen to align with the fields of Le Borgne et al. (2008a), Le Borgne et al. (2008b), which first introduced the SMM. After generating

the permeability field, we then calculate our flow field by solving Darcy's law with incompressibility

$$\mathbf{v}(\mathbf{x}) = -\frac{\kappa(\mathbf{x})}{\mu}\nabla p, \qquad \nabla \cdot \mathbf{v} = 0, \tag{1}$$

using a finite volume method Aarnes et al. (2007), where $\mathbf{v}(\mathbf{x})$ is the velocity $[LT^{-1}]$, p is the pressure $[ML^{-1}T^{-2}]$, and μ is the viscosity $[ML^{-1}T^{-1}]$. We impose a constant head value at both the upstream and downstream boundaries and a no flux condition on the boundaries parallel to the flow. The flow domain was generated to be large enough such that the reactive solutes do not interact with the boundaries throughout our simulations. Domain lengths of $L_x = 4000\lambda$ and $L_y = 1000\lambda$ in the x and y directions were acceptable for this purpose. The natural log of the permeability field and the natural log of the absolute value of the velocity $v = \sqrt{v_x^2 + v_y^2}$ are shown in Fig. 1. An advection dominated system is examined here with a Péclet number equal to $Pe = \frac{\overline{v_x}\lambda}{D} = 200$, where $\overline{v_x} = 1$ is the mean velocity in the horizontal direction of the flow and $D = 10^{-2}$ is the constant dispersion coefficient.While all parameters here are intentionally presented in dimensionless format, this Péclet number is representative of a realistic system. For example, an aquifer with a mean velocity of $1e-5m/s$, a correlation length of $2m$, and a dispersion coefficient of $1e-7m^2/s$, all physically reasonable numbers, will have a Péclet number of 200.

We consider a system with A and B initially separated by a sharp interface. The reactive solutes A and B are discretized into a large number of particles N that each represent some amount of mass of the solute m_p. Here, $N = 1e6$ is the total number of particles in the system, with $N_A = N_B = 5e5$ particles for each reactive solute. The reactive solute B is located over a rectangular area from $0.4L_x$ to $0.4L_x + 10L_{cell}$ in the x direction and from $0.45L_y$ to $0.55L_y$ in the y direction, where $L_{cell} = 24\lambda = 48$ is the Spatial Markov model cell length. The reactive solute A is located over a rectangular area from $0.4L_x + 10L_{cell}$ to $0.4L_x + 20L_{cell}$ in the x direction and from $0.45L_y$ to $0.55L_y$ in the y direction. Owing to this choice the solute samples a relevant portion of the domain, being the dimension of area initially occupied by the solute much larger than the characteristic correlation length of the conductivity and velocity fields. The particles are flux weighted over their initial rectangular area such that larger numbers of particles are present in higher velocity regions. The initial location of the reactive solutes A and B are depicted on Fig. 1.

The governing equation for bimolecular reactive transport in this system is the advection dispersion reaction equation (ADRE)

$$\frac{\partial C_i}{\partial t} = D\nabla^2 C_i - \mathbf{v}\cdot\nabla C_i - kC_A C_B \qquad i = A, B \tag{2}$$

where C_i is the reactive solute concentration [mol L^{-2}], D is the constant local dispersion coefficent $[L^2T^{-1}]$, and k is the reaction rate constant $[L^2\ \text{mol}^{-1}T^{-1}]$. It should be noted that we are considering a constant local dispersion coefficient for both A and B here, but in reality different chemical species would have different dispersion coefficients. This choice of dispersion coefficient impacts the overall mixing in the system and therefore chemical reaction Rolle et al. (2013). While we make the simplification of keeping the dispersion coefficient constant for A and B here, this method could easily be extended to consider unique dispersion coefficients for different chemical species and this is something that should be considered in future works. In this study, we will model Eq. 2 using a fully resolved reactive random walk method described in Sect. 3 and attempt to replicate these results by extending the upscaled LATERS Markov model to this system.

3 Fully resolved model: Reactive random walk

In this section, we will describe the fully resolved reactive random walk method that was first developed by Benson and Meerschaert (2008) and will be used to evaluate the upscaled model. We consider a single realization of log-permeability, i.e. we consider the field to be known and deterministic. We neglect then parametric uncertainty,

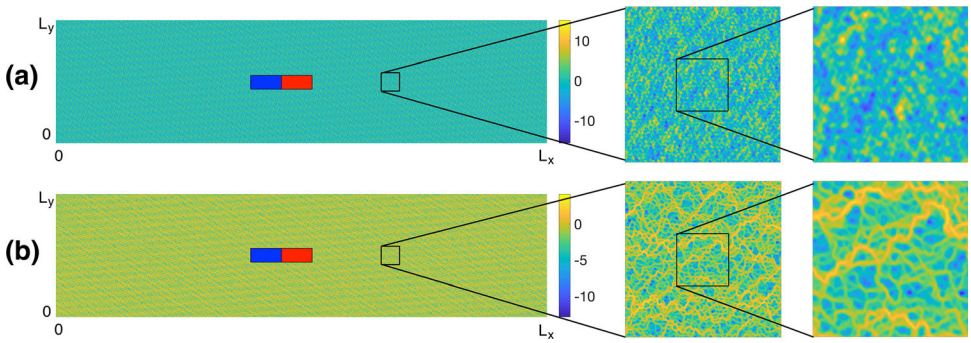

Fig. 1 (**a**) The natural log of the permeability field κ and (**b**) the natural log of the absolute value of the velocity $v = \sqrt{v_x^2 + v_y^2}$, where v_x and v_y are the velocity fields in the horizontal and vertical flow directions. The red and blue boxes indicate the initial locations of the reactive solutes A and B, respectively

typically acknowledged by considering ensembles of statistically equivalent multiple realization of $\ln\kappa$ and focus instead on the quantification of model error introduced by reduced complexity (or upscaled) approaches. Our analysis considers the fully resolved simulation of Eq. (2) as ground truth, against which we will compare the proposed upscaling approaches, described later in Sect. 4.3. A summary of the algorithm used for the fully resolved simulation will be provided here and more detailed information can be found in Benson and Meerschaert (2008), Paster et al. (2013), Paster et al. (2014). In this fully resolved reactive random walk method, time is discretized into time steps of size $\Delta t = 0.01$. The time step size was selected following a convergence test.

At each time step in this model, reactions and transport are simulated in separate steps by operator splitting. We begin with the reactive step by determining which particles, if any, will react during the current time step. The probability of reaction is determined by both the kinetics of the reaction and the ability of the particles to come into contact. It is defined as

$$P_{reaction} = P_{coll} P_{react|coll} \tag{3}$$

where P_{coll} is the probability that particles initially separated by some distance s will come into contact over the time step Δt and $P_{react|coll}$ is the probability that the particles will react once they have come into contact. The probability of collocation is given by

$$P_{coll} = \frac{1}{8\pi D\Delta t} e^{-\frac{s^2}{8D\Delta t}} \tag{4}$$

and the probability of reaction given collocation is defined as

$$P_{react|coll} = k m_p \Delta t, \tag{5}$$

where k is the reaction rate constant and m_p is the particle mass. To determine which particles will react, we determine which B particles are within some defined radius of each A particle. This search radius is selected such that the probability of reaction for each A particle with any B particle outside of this radius is less than 10^{-6}, which has been shown to give acceptable results Paster et al. (2014). This radius is defined by

$$r = \sqrt{-8D\Delta t \log\left(\frac{8\pi D\Delta t P_{react,thr}}{P_{react|coll}}\right)} \tag{6}$$

where $P_{react,thr} = 10^{-6}$ is a numerical threshold, set to balance efficiency and accuracy of the algorithm. To make the particle searching process more computationally efficient, a k-d tree is implemented using the KDTreeSearcher function in MATLAB to reduce complexity from an $O(N^2)$ process to an $O(N\log N)$ process. Once we have obtained a list of B particles that are within the defined search radius of each A particle, we calculate the probability of reaction $P_{reaction,i}$ and draw a random number $\eta_i \sim U(0,1)$ for each AB particle pair. If $P_{reaction} > \eta_i$ for any AB pair, then the two A and B particles react with one another and are removed from the system according to the reaction $A + B \rightarrow \emptyset$. If more than one B particle meets the requirement for reaction with a single A particle, then the AB pair with the largest value of $P_{reaction,i} - \eta_i$ is selected for reaction. If no B particle meets the reaction requirement for a single A particle, then that A particle does not react during this time step.

Once the reaction component is completed, we move on to transport. In a single time step, each particle moves forward in time some amount Δt and moves in space according to the Langevin equation

$$\mathbf{x}(t + \Delta t) = \mathbf{x}(t) + \mathbf{v}(t)\Delta t + \sqrt{2D\Delta t}\,\xi, \tag{7}$$

where $\mathbf{x}$ is the particle's position vector, $\mathbf{v}$ is the particle velocity determined from the underlying flow fields, $\xi \sim N(0,1)$, and $\sqrt{2D\Delta t}\,\xi$ represents a random jump due to dispersion with zero mean and a variance equal to $2D\Delta t$.

4 Upscaled model: LATERS Markov model

The LATERS Markov model was developed by Sund et al. (2017) to predict effective bimolecular reactive transport in a relatively simple two-dimensional porous medium consisting of flow around an array of solid cylinders. Here, we aim to extend this work to upscale reactive transport in more general flows through heterogeneous porous media. This method is a hybrid Lagrangian-Eulerian model that combines the stochastic SMM to predict transport and a volume averaged reaction rate equation to predict reaction.

4.1 Parameterization of the LATERS Markov model

The LATERS Markov model is parameterized by running high resolution particle tracking simulations over two representative cells of the flow of length $L_{cell} = 24\lambda$, where λ is the correlation length of the permeability field. This cell length and the flow field are selected to match Wright et al. (2019). In our high resolution particle tracking simulation, we discretize time into small time steps of size $\Delta t = 0.01$ and move the particles by random walk at each time step according to Eq. 7. As discussed in Sect. 2, our initial condition is to have flux-weighted A and B particles initially separated by a sharp interface. If $\mathbf{x_0}(x, y)$ is the vector of the initial A and B particle locations, we run the high resolution particle tracking simulations as the particles

travel from $x_0(x,y)$ to $x_0(x,y)+2L_{cell}$ in the x-direction and record the following information:

- τ_1 - the time it took for a particle to travel through the first cell
- τ_2 - the time it took for a particle to travel through the second cell
- y_0 - the particle's y position at the inlet of the first cell
- y_1 - the particle's y position at the inlet of the second cell.

This joint distribution $f(\tau_1,\tau_2,y_0,y_1)$ is then used to inform the upscaled model. The original SMM parameterization only required the joint distribution $f(\tau_1,\tau_2)$ Le Borgne et al. (2008a), Le Borgne et al. (2008b), but the added information of y_0 and y_1 are needed here to predict mixing.

4.2 Lagrangian transport: Spatial Markov model

In each step of the baseline SMM, particles move forward in time and space according to the Langevin equation

$$\begin{aligned} x^{(n+1)} &= x^{(n)} + L_{cell} \\ t^{(n+1)} &= t^{(n)} + \tau^{(n+1)} \quad n = 0,1,2,... \end{aligned} \tag{8}$$

where $\tau^{(n+1)}$ is sampled from the distribution $f(\tau)$ defined by

$$f(\tau) = \begin{cases} f(\tau_1) & \text{if } n = 0 \\ f(\tau^{(n+1)}|\tau^{(n)}) & \text{if } n = 1,2,\ldots. \end{cases} \tag{9}$$

The distribution $f(\tau_1)$ is recorded during the parameterization step and $f(\tau^{(n+1)}|\tau^{(n)})$ is approximated using a transition matrix. The transition matrix is created by first separating $f(\tau_1)$ into a number of equiprobable bins N_T and recording the cutoff times associated with each bin. Bin 1 corresponds to the particles with the fastest travel times and Bin N_T corresponds to the bin with the slowest travel times. $N_T = 20$ was selected following a convergence test and is within the appropriate range of bin numbers determined by Le Borgne et al. (2011). A particle's travel time τ_p is in Bin i if $t_{c,i} \le \tau_p < t_{c,i+1}$, where $t_{c,i}$ is the cutoff time for Bin i, $t_{c,1} = 0$, and t_{c,N_T+1} is greater than the maximum value of τ_1 and τ_2 recorded during the parameterization step. The transition matrix is then defined as

$$T_{i,j} = P(\tau_2 \in \text{Bin}\, j | \tau_1 \in \text{Bin}\, i) \approx f(\tau_2|\tau_1), \tag{10}$$

where it is assumed that $f(\tau^{(n+1)}|\tau^{(n)}) = f(\tau_2|\tau_1)$. Therefore, each block of the transition matrix $T_{i,j}$ gives the probability that a particle will have a travel time in Bin j given that its travel time was in Bin i in the previous step.

From the traditional SMM described above, we know which cell each particle is in at any time t^*, how long it has been in that cell, and how long it will remain in that cell. The exact location of the particle within the cell is unknown. Several downscaling procedures within the upscaled SMM were developed by Wright et al. (2019) to predict particle locations at any time t^* for the purpose of quantifying mixing. Here, it is necessary to quantify how the reactive solutes A and B mix relative to each other in order to accurately account for reaction. To this end we employ the downscaling methods that were developed in Wright et al. (2019) to predict particle locations at specific times of interest. These particle locations can then be mapped onto a grid to generate concentration fields for the purpose of calculating reactions.

4.3 Predicting sub-cell particle locations

Wright et al. (2019) developed several methods to extend the SMM to predict mixing. The goal of this work was to develop downscaling procedures within the upscaled SMM that can select particle locations (x^*,y^*) at any time t^* that can be used to generate concentration fields able to accurately quantify mixing. These downscaling methods are briefly summarized here and more details can be found in Wright et al. (2019).

In each of these downscaling procedures it is known that at any time t^* each particle is located in some Cell $n+1$, where n is the SMM step number. The downscaled x locations of the particles are selected within their respective SMM cells at time t^* by assigning to each particle a mean longitudinal velocity through the cell equal to $\overline{v^{(n+1)}} = L_{cell}/\tau^{(n+1)}$, where L_{cell} is the SMM cell length and $\tau^{(n+1)}$ is the particle's travel time through the cell. We then assume that each particle moves straight across Cell $n+1$ with a uniform velocity equal to $\overline{v^{(n+1)}}$ and linearly interpolate along this path to determine x^*, i.e.

$$x^* = (t^* - t^{(n)})\overline{v^{(n+1)}} + x^{(n)}. \tag{11}$$

This is the same choice for predicting x locations as in Sund et al. (2017).

Four different methods were considered to select the downscaled particle y locations:

- Method 0

  In Method 0, the y^* positions of the particles are selected randomly with uniform probability between the initial maximum and minimum particle y values, y_{max} and y_{min}. Thus, the y positions predicted by Method 0 are given by

  $$y^* = (y_{max} - y_{min})\eta^* + y_{min} \tag{12}$$

  where $\eta^* \in U(0,1)$. This choice may be made in a system where no information is available on probable y positions or the particle y locations are unimportant.

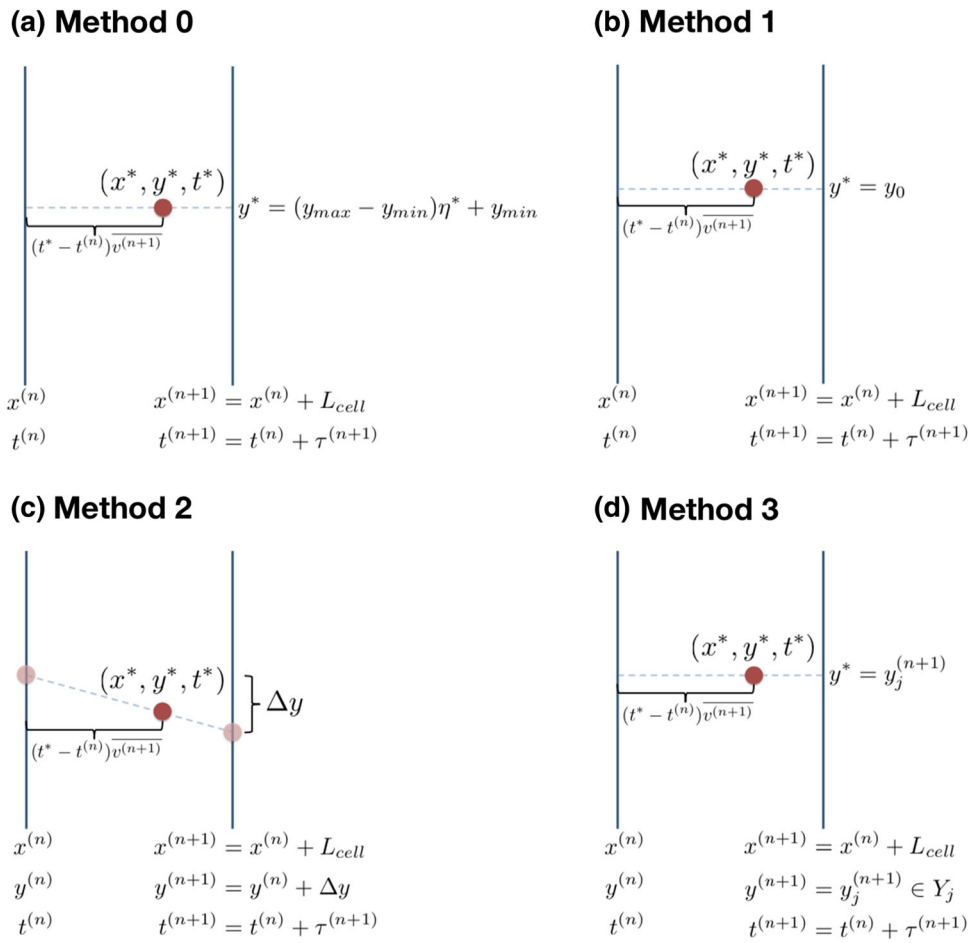

Fig. 2 Illustrations of the downscaling procedures Methods 0, 1, 2, and 3 in a single SMM cell

This method is illustrated for a particle located in Cell $n+1$ in Fig. 2a.

- Method 1
  The y^* locations for Method 1 are selected to be equal to each particle's initial y position at all times, i.e.

$$y^* = y_0. \tag{13}$$

This corresponds to the idea that a particle's initial position might be its most likely location and may be a sufficient approximation at all times. An illustration of this method for a particle located in Cell $n+1$ can be found in Fig. 2b.

- Method 2
  In an effort to simulate a more realistic particle trajectory, Method 2 involves adding a y-component to each SMM step, i.e.

$$\begin{aligned} x^{(n+1)} &= x^{(n)} + L_{cell} \\ y^{(n+1)} &= y^{(n)} + \Delta y \\ t^{(n+1)} &= t^{(n)} + \tau^{(n+1)} \end{aligned} \qquad \text{n = 0,1,2,....} \tag{14}$$

Here, $\Delta y = y_0 - y_1$, where y_0 and y_1 were measured during the parameterization step. Each travel time τ_1 from the model parameterization has a corresponding Δy value that was measured. The travel times $\tau^{(n+1)}$ are selected as usual with the transition matrix by Eq. 9 and the corresponding Δy values are chosen. The downscaled y positions are then determined by linearly interpolating between $y^{(n)}$ and $y^{(n+1)}$ to the location x^*, i.e.

$$y^* = \frac{y^{(n+1)} - y^{(n)}}{L_{cell}}(x^* - x^{(n)}) + y^{(n)}. \tag{15}$$

This method is illustrated in Fig. 2c for a particle located in Cell $n+1$.

- Method 3
  In Method 3, the parameterization step is adjusted to incorporate more information on particle trajectories. The parameterization step previously recorded the joint distribution $f(y_0, y_1, \tau_1, \tau_2)$; here, it is extended to measure $f(y_0, y_{t,1}, y_{t,2}, ..., y_{t,N_t} = y_1, \tau_1, \tau_2)$, where $y_{t,\#}$ are particle y locations measured at N_t points along each particle trajectory through the first parameterization cell. The particle trajectories are separated into a

number N_z of equiprobable zones based on their initial y position y_0. $N_t = 20$ and $N_z = 20$ were found to be satisfactory numbers of trajectory points and zones Wright et al. (2019). Then, a set of possible y values, Y_j, is generated for each zone number j. Y_j contains all of the y values measured along the trajectories of particles that had y_0 in Zone j. Finally, the downscaled y position is given by

$$y^* = y_j^{(n+1)}, \tag{16}$$

where $y_j^{(n+1)}$ is a y value selected randomly at each SMM step from the set Y_j associated with each particle's zone number j. Each particle's zone number is selected based on their initial y position, y_0, and does not change for the duration of the simulation. This method is illustrated in Fig. 2d for a particle located in Cell $n + 1$.

Once the locations of all particles are predicted, they can be mapped onto a grid to generate the concentration fields of the reactive solutes A and B that will be used to calculate the amount of reaction that takes place. The concentration grid is obtained by discretizing the flow domain into cells of size $l_{x,C}$ in the streamwise direction and $l_{y,C}$ in the spanwise direction and calculating the amount of mass (i.e. the number of particles of mass m_p) in each grid cell of area $A_{C\,grid} = l_{x,C}\, l_{y,C}$.

Our initial condition is to have the reactive solutes A and B initially separate as indicated on Fig. 1. To determine which downscaling method developed in Wright et al. (2019) and summarized in Sect. 4.3 is best suited for this setup, we calculate the integral of the squared concentration for the corresponding conservative setup. That is, we measure $M = \int C^2(\mathbf{x}, t)d\mathbf{x}$ in time for non-reactive particles at the same initial positions as the A and B particles. This mixing metric, M, was chosen as it was previously used to quantify mixing in Wright et al. (2019) where these downscaling methods were first developed. Fig. 3 shows M vs. time calculated using each of the downscaling methods described in Sect. 4.3 and the fully resolved model. To obtain this calculation, particle locations are predicted by each of the downscaling methods. These particle locations are then mapped onto a grid to generate a concentration field for each method and the integral of the squared concentration is computed. The results of the upscaled model calculations are then compared to the results of the fully resolved model. From a qualitative analysis of Fig. 3, it is clear that Method 1 provides the best estimate of mixing for this setup. For this reason, this is the method that is selected to predict particle locations for the present implementation of the LATERS

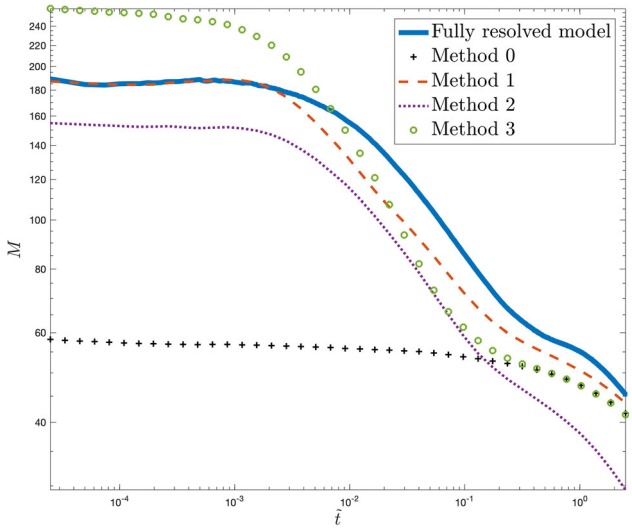

Fig. 3 The integral of the squared concentration M vs. time for the downscaling methods developed in Wright et al. (2019) for predicting concentration fields

Markov model. Thus, our particle locations at time t^* are selected by

$$\begin{aligned} x^* &= (t^* - t^{(n)})\overline{v^{(n+1)}} + x^{(n)} \\ y^* &= y_0. \end{aligned} \tag{17}$$

It should be noted that this result for best downscaling method differs from the results of Wright et al. (2019) where Method 3 was the most successful. This is due to the different initial condition used in this setup. A flux-weighted line injection was considered in Wright et al. (2019), while particles are flux-weighted here across an area with a length of $20L_{cell}$ and a width of $0.1L_y$. Method 3 is unable to prevent particles from crossing paths with one another, an effect that is amplified in this initial condition compared to the results with a flux-weighted line injection. Method 2 overpredicts mixing at all times for the same reason, but interestingly appears to accurately predict the rate of change of the mixing metric M in Fig. 3.

4.4 Eulerian reaction: volume averaged reaction rate equation

In the LATERS Markov model, time is discretized into steps of size dt. Here, dt = 0.1 ($\widetilde{dt} = 2.5 \cdot 10^{-4}$) is selected, which meets the requirement of Sund et al. (2017) that the time step be at least ten times smaller than the fastest travel time measured during the model parameterization. Time is non-dimensionalized here by a dispersion time scale defined as $t_D = \frac{\lambda^2}{D}$, i.e. $\widetilde{t} = t/t_D$, where the tilde indicates the quantity is non-dimensionalized. This upscaled model time step dt is also ten times larger than the fully resolved

model time step $\Delta t = 0.01$ ($\widetilde{\Delta t} = 2.5 \cdot 10^{-5}$). After obtaining the concentration fields of the reactive solutes by predicting particle locations at any time t^* as described in the previous section, the next step in the LATERS Markov model is to calculate how much reaction should occur in the system during this model step between times $t^* - dt$ and t^* and remove the mass of the reactive solutes A and B accordingly.

If the ADRE given by Eq. 2 is volume averaged, the reaction term is found to be

$$\langle r \rangle = k\left[\langle C_A \rangle \langle C_B \rangle + \left\langle C'_A C'_B \right\rangle\right] \tag{18}$$

where the volume average $\langle \bigstar \rangle$ is defined by

$$\langle \bigstar \rangle = \frac{1}{V_f} \int_{V_f} \bigstar \, dV, \tag{19}$$

V_f being the volume of the fluid being averaged. Fluctuations are then defined as

$$\bigstar' = \bigstar - \langle \bigstar \rangle. \tag{20}$$

To compute the volume averaged terms $\langle C_A \rangle$, $\langle C_A \rangle$, and $\left\langle C'_A C'_B \right\rangle$ required for calculating $\langle r \rangle$ according to Eq. 18, we must define a reaction grid where each grid cell represents the averaging volume V_f and has cell lengths of $l_{x,r}$ in the streamwise direction and $l_{y,r}$ in the spanwise direction. The area of the reaction volume has a size of $V_f = l_{x,r}\, l_{y,r}$ in our two-dimensional system. It is a requirement for these calculations that the reaction grid has a coarser resolution than the concentration grid and that $N_{grid,x} = l_{x,r}/l_{x,C}$ and $N_{grid,y} = l_{y,r}/l_{y,C}$ are integers. Thus, each reaction volume V_f contains a number of concentration grid cells equal to $N_{C\,cells} = N_{grid,x} N_{grid,y}$. We will consider here a reaction grid with resolution $l_{x,r} = l_{y,r} = L_{cell} = 24\lambda = 48$, so that the reaction volume coincides with the upscaled cell volume. $\langle C_A \rangle$ and $\langle C_A \rangle$ are then calculated in each reaction volume according to Eq. 19 and the fluctuation term $\left\langle C'_A C'_B \right\rangle$ is calculated by defining $C'_A = C_A - \langle C_A \rangle$ and $C'_B = C_B - \langle C_B \rangle$ according to Eq. 20 and using Eq. 19.

After calculating $\langle r \rangle$, the change of concentration due to reaction within a defined volume V_f is given by

$$\Delta \langle C_i \rangle = -\langle r \rangle dt \qquad i = A, B, \tag{21}$$

where dt is the time step size. The amount of mass to be removed from the reaction volume V_f is then

$$\Delta m = \Delta \langle C_i \rangle V_f. \tag{22}$$

To determine which particles within a given reaction volume will react, the probability of reaction is calculated for both the reactive solutes A and B. This probability of reaction is given by

$$P_{reaction,i} = \frac{\Delta m}{M_{V_f,i}} \qquad i = A, B, \tag{23}$$

where $M_{V_f,i}$ is the total mass of A or B within the reaction volume. A random number $\xi \sim U(0,1)$ is then drawn for each A and B particle within the reaction volume and a particle will react if $P_{reaction,i} > \xi$. The particles that are selected for reaction are then removed from the system according to the reaction $A + B \rightarrow \emptyset$.

5 Results

The LATERS Markov model and the fully resolved model were run for a range of Damköhler numbers equal to $Da =$ 0.625, 6.25, and 62.5. The Damköhler number is defined here with a dispersion time scale and a length scale equal to the correlation length of the permeability field, i.e. $Da = \frac{kC_0\lambda^2}{D}$. Low Da indicates that reactions are happening more slowly relative to mixing by dispersion and behavior that is nearer to well-mixed is anticipated. In contrast, high Da corresponds to a system where reactions are happening more quickly relative to mixing by dispersion and stronger incomplete mixing effects are expected. As mentioned previously, we will consider an advection-dominated system with a Péclet number of $Pe = 200$ for all of these Da numbers under consideration.

The total mass of the reactive solute B in the system versus time for $Da =$ 0.625, 6.25, and 62.5 is shown in Fig. 4. It is observed in Fig. 4 that the LATERS Markov model predicts the total reactant mass in the system very

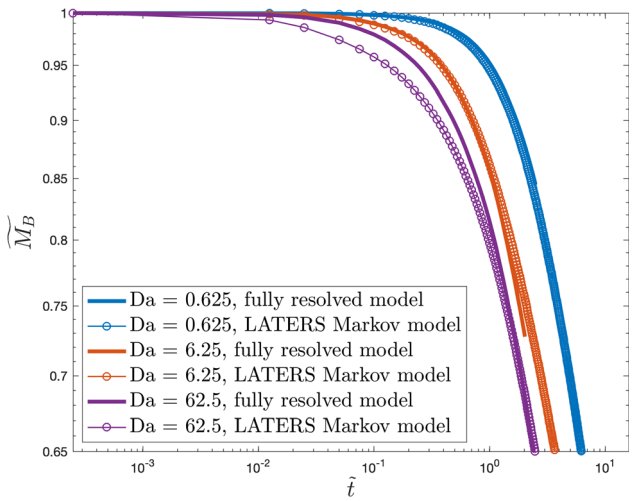

Fig. 4 The total mass of B in the domain normalized by the total mass of B in the domain at time = 0, i.e. $\widetilde{M_B} = M_B/M_{B,0}$ vs. time for $Da =$ 0.625, 6.25, and 62.5. Time is non-dimensionalized by a dispersion time scale defined as $\frac{\lambda^2}{D}$, where λ is the correlation length of the natural log of the permeability field and D is the constant dispersion coefficient

well for $Da = 0.625$ and 6.25 relative to the fully resolved model, while the LATERS Markov model overestimates reaction for $Da = 62.5$. This indicates that upscaled LATERS Markov model might not be as successful in systems where incomplete mixing effects are important at least with the currently assumed discretization.

To examine this further, we look at the spatial distribution of reactant concentrations. Figs. 5, 6, and 7 show the volume averaged concentrations of A and B in each reaction cell averaged across the domain in the y-direction versus x at three different times throughout the simulation for $Da = 0.625$, 6.25, and 62.5, respectively. Figs. 5 and 6 show that the LATERS Markov model is doing a good job of predicting the location of the reactive solutes in the streamwise direction for both $Da = 0.625$ and 6.25, respectively, and demonstrate that the appropriate amount of reaction is happening in the interface region where the reactive solutes A and B overlap in these systems. In contrast, Fig. 7 demonstrates that too much reaction is occuring in the interface between the solutes A and B for the $Da = 62.5$ case, which is consistent with the overprediction of reaction observed in Fig. 4.

To illustrate the system more qualitatively we examine the locations of the solutes A and B. Figure 8 shows the A and B particle locations at $\tilde{t} = 2.5$ in our upscaled LATERS Markov model and fully resolved simulations for $Da = 0.625$, 6.25, and 62.5. It is important to note here that we are not trying to exactly replicate the particle locations of the fully resolved model with our upscaled model, but instead accurately capture the amount of mixing between the A and B particles in order to correctly predict reaction. From Fig. 8, it appears that the A and B particles in the upscaled model are almost completely depleted by reaction in the interface region for the $Da = 62.5$ case, limiting the ability of A and B particles to further mix and react. This is consistent with what is observed in Figs. 7 and 8c indicates that reactions occur too quickly at the interface between the solutes A and B in the upscaled model for the $Da = 62.5$ case. Then, after the interface region is depleted by reaction, a slowdown of reactions is observed due to the fact that A and B particles are more limited in their ability to come into contact. This result is consistent with Fig. 4, which shows an over-prediction of reaction in the upscaled model for $Da = 62.5$ relative to the fully resolved model. This is followed by a self-correction: the depletion at the

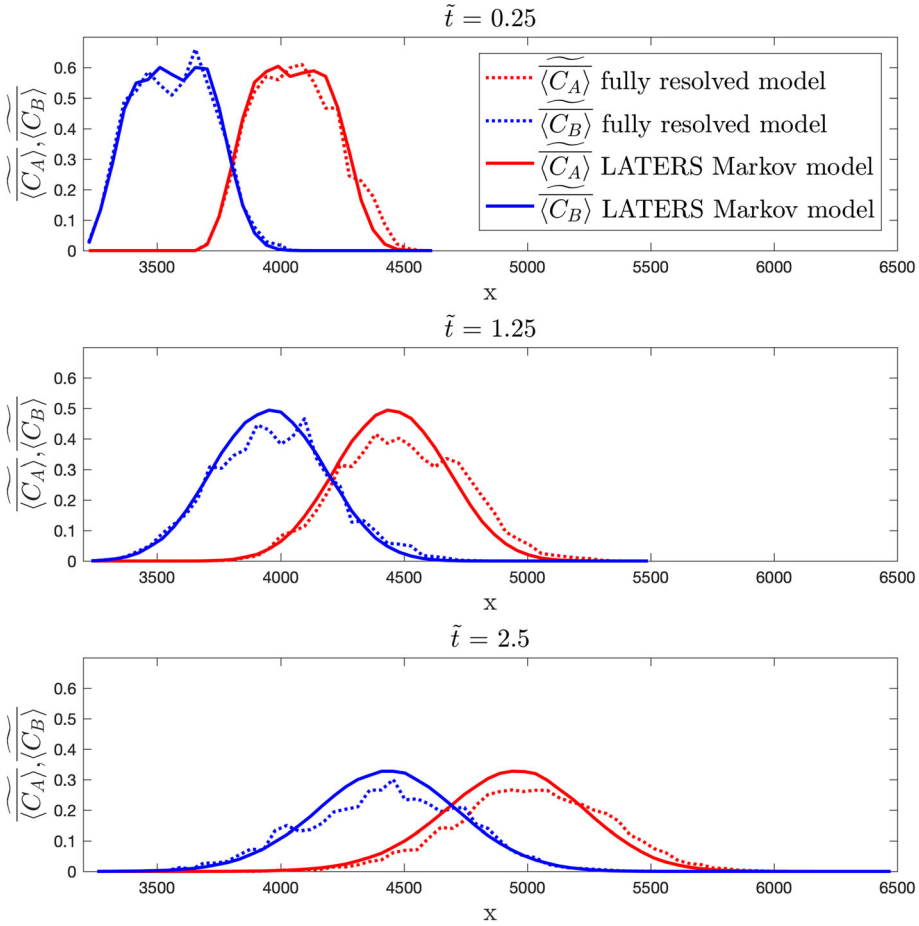

Fig. 5 $\widetilde{\langle C_A \rangle}$ and $\widetilde{\langle C_B \rangle}$ vs. x at times $\tilde{t} = 0.25$, 1.25, and 2.5 for $Da = 0.625$. The overbar indicates an average across the reaction cells in the y-direction and $\langle \bigstar \rangle$ indicates a volume average over a single reaction cell

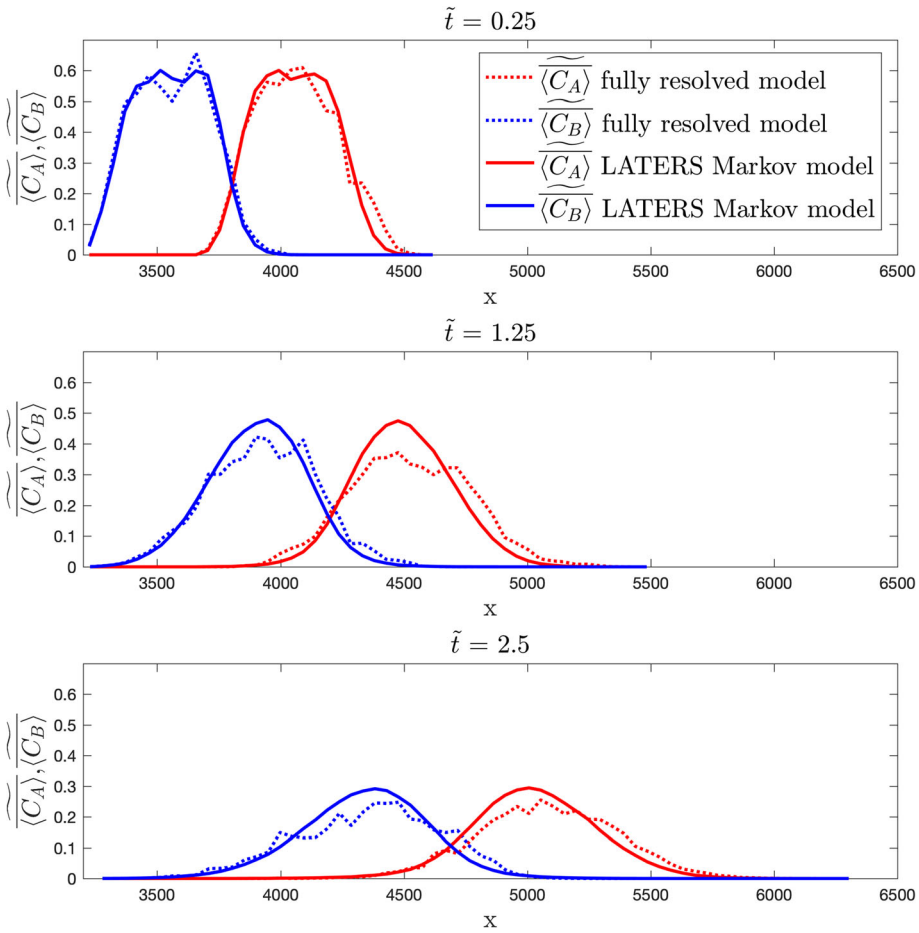

Fig. 6 $\widetilde{\langle C_A \rangle}$ and $\widetilde{\langle C_B \rangle}$ vs. x at times $\tilde{t} = 0.25$, 1.25, and 2.5 for $Da = 6.25$. The overbar indicates an average across the reaction cells in the y-direction and $\langle \bigstar \rangle$ indicates a volume average over a single reaction cell

interface causes a slowdown of reactions that results in the upscaled model ultimately returning to match the amount of the reactive solute mass B from the fully resolved model at later times.

6 Discussion

In this section, we examine more closely the shortcomings of the LATERS Markov model at high Damköhler numbers. Since this method works well for lower Da when the system is behaving closer to well-mixed, we focus here on the $Da = 62.5$ case.

We address three main questions regarding the cause of the over-prediction of reactions for the $Da = 62.5$ case. First, in Sect. 6.1 we test whether or not the magnitude of the fluctuation term in the volume averaged reaction rate equation, $\langle C'_A C'_B \rangle$, is too small. This fluctuation term represents the amount of incomplete mixing in the system. If $\langle C'_A C'_B \rangle$ is not accounted for properly, it could explain why the LATERS Markov model predicts too much reaction for $Da = 62.5$. Second, we determine how the upscaled model is affected by grid resolution. The LATERS Markov model requires discretizing the domain into two separate grids: one to calculate the concentration fields of the reactive solutes A and B and the other to calculate reactions. In the previous section, we showed results for a concentration grid comprised of square grid cells with edges of length $l_{x,C} = l_{y,C} = \lambda$ and a reaction grid with square grid cells of size $l_{x,r} = l_{x,r} = L_{cell}$. These grid resolutions were a natural choice as they were based on the correlation length of the permeability field, λ, and the SMM cell length, L_{cell}, which are physical length scales that characterize the system. In Sect. 6.2, we examine the impact of these grid resolutions on upscaled reactive transport. Finally, we explore the effect of the mass reduction method used to account for reaction within a reaction volume and its impact on the system in Sect. 6.3.

6.1 Is the magnitude of fluctuation term in the volume averaged reaction rate equation too small?

In this section, we aim to identify whether or not the magnitude of the fluctuation term, $\langle C'_A C'_B \rangle$, in the volume

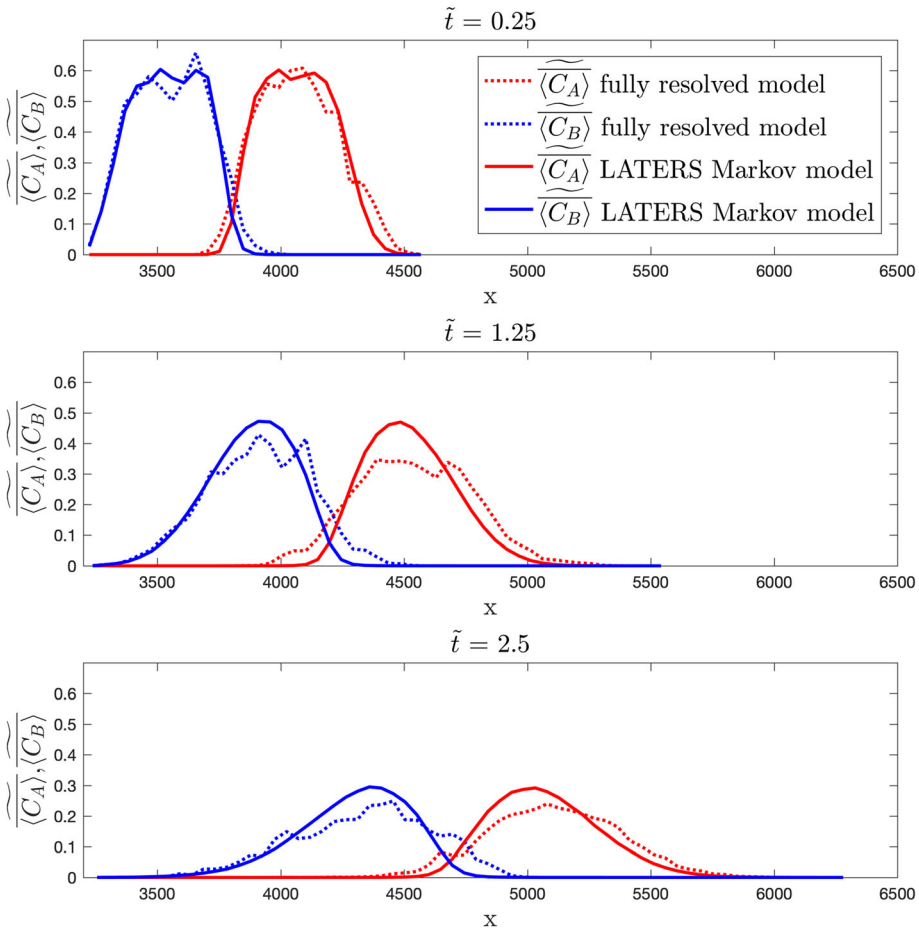

Fig. 7 $\widetilde{\langle C_A \rangle}$ and $\widetilde{\langle C_B \rangle}$ vs. x at times $\tilde{t} = 0.25$, 1.25, and 2.5 for $Da = 62.5$. The overbar indicates an average across the reaction cells in the vertical direction and $\langle \bigstar \rangle$ indicates a volume average over a single reaction cell

averaged reaction rate equation given by Eq. 18 is too small. This term should account for the slowdown in reaction due to incomplete mixing. If the magnitude of $\langle C_A' C_B' \rangle$ is not sufficiently large, it might be responsible for the over-prediction of reaction that was observed for the $Da = 62.5$ case. To begin, we run the LATERS Markov model without the fluctuation term, i.e. with a volume averaged reaction rate equation given by

$$\langle r \rangle = k \langle C_A \rangle \langle C_B \rangle, \tag{24}$$

which says that the reaction rate is simply based on the average concentrations. The total mass of the reactive solute B for the upscaled model run with Eq. 24, the original upscaled model run with Eq.Eq. 18, and the fully resolved model versus time are shown in Fig. 9. From this Figure, it is observed that the results for the original LATERS Markov model simulation and the new upscaled simulation without the fluctuation term in the volume averaged reaction rate equation are nearly identical. This suggests that the approximation of the fluctuation term in Eq. 18 has almost no effect on the upscaled system.

To further examine this, we explore what happens to the system if the magnitude of the fluctuation term $\langle C_A' C_B' \rangle$ is increased. We run the LATERS Markov model with three variations of Eq. 18 given by

$$\langle r \rangle = k \left[\langle C_A \rangle \langle C_B \rangle + \alpha \langle C_A' C_B' \rangle \right], \tag{25}$$

where α = 1.1, 2, and 5. By manually increasing the fluctuation term by factors of 1.1, 2, and 5, we can quantify the impact of larger values of $\langle C_A' C_B' \rangle$ on the system.

Figure 10a shows the total mass in the domain versus time for the fully resolved reactive random walk model and the LATERS Markov model using Eq. 25 with α = 1, 1.1, 2, and 5. The case with $\alpha = 1$ is the original volume averaged reaction rate equation given by Eq. 18 and the results were shown previously in Sect. 5. It is observed that increasing the fluctuation term by factors of $\alpha = 1.1$ and 2 has little effect on the results. For $\alpha = 5$, we observe a slowdown of reactions between $\sim \tilde{t} = 4 \cdot 10^{-2}$ and $2 \cdot 10^{-1}$ relative to the other upscaled model results. During this time frame, the predicted reaction rate of the LATERS Markov model with $\alpha = 5$ is reduced and approaches the fully resolved simulation results until approximately $\tilde{t} = 2 \cdot 10^{-1}$. This slowdown in reactions is anticipated, as the fluctuation term in Eq. 25 represents the reduction in the amount of reaction due to incomplete mixing.

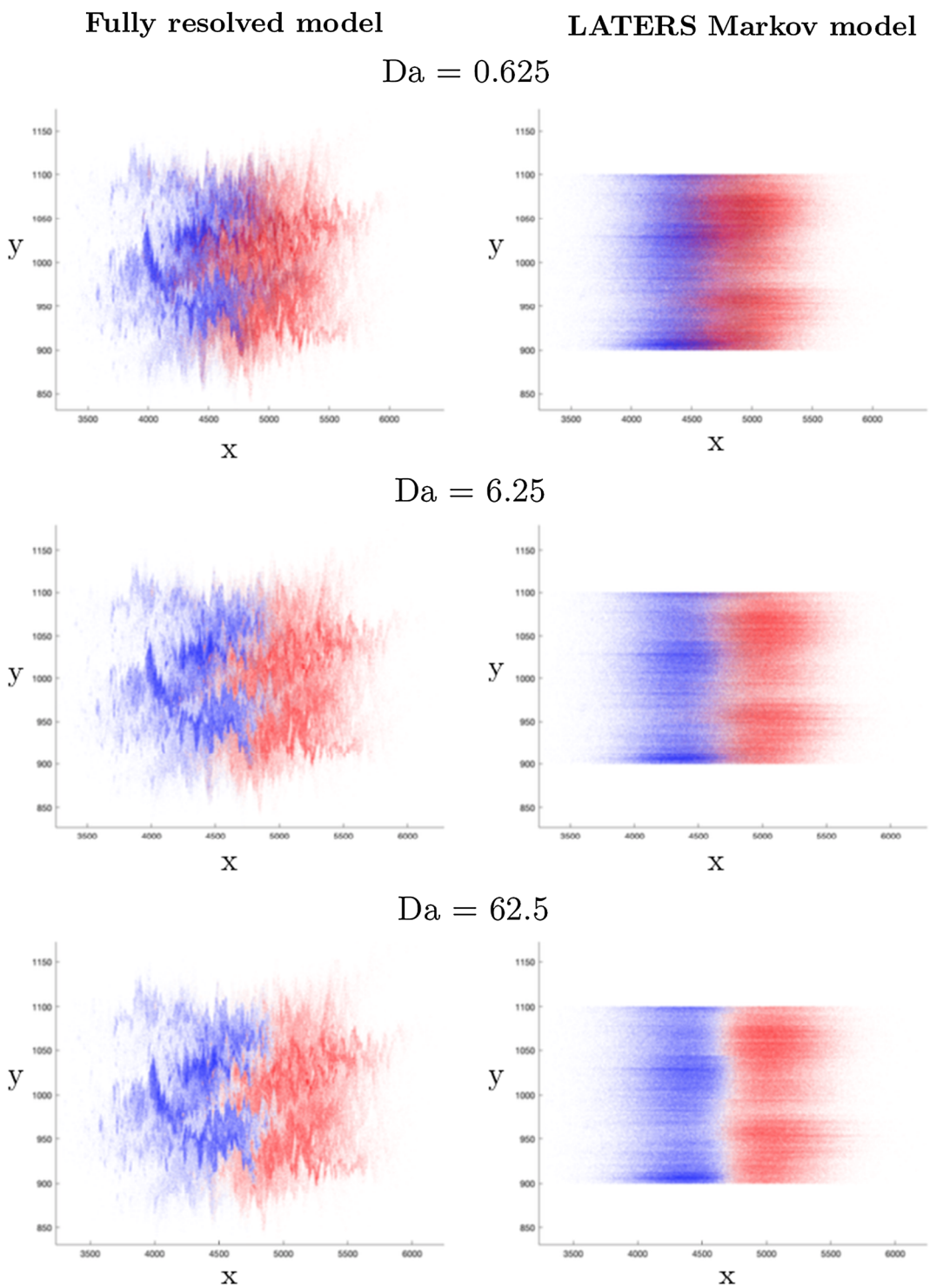

Fig. 8 The locations of the particles at times $\tilde{t} = 2.5$ for $Da = 0.625$, 6.25, and 62.5 from the fully resolved model and LATERS Markov model simulations

However, after time $\tilde{t} = 2 \cdot 10^{-1}$, the upscaled model with $\alpha = 5$ increases its reaction rate and the simulation results revert back towards the other upscaled model predictions with $\alpha = 1$, 1.1, and 2. To determine the cause of this shift from a slow down of reactions back to faster reactions, we examine the terms in Eq. 25 more closely.

Figure 10b-d shows the sum over the domain of the mean and fluctuation terms from Eq. 25, $\langle C_A \rangle \langle C_B \rangle$ and

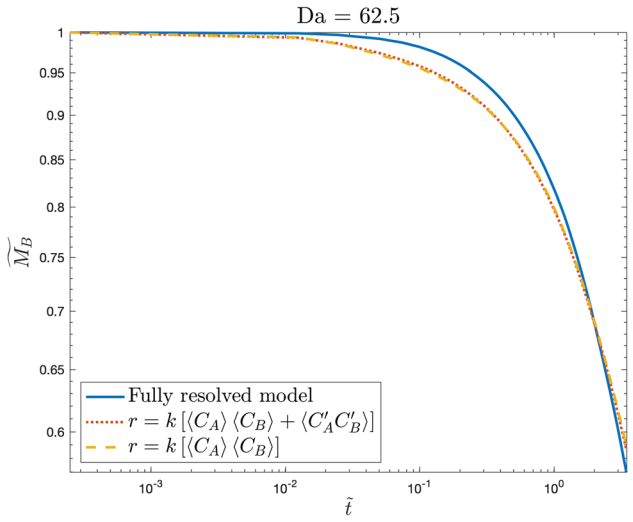

Fig. 9 The total mass of B in the domain normalized by the total mass of B in the domain at time = 0, i.e. $\widetilde{M_B} = M_B/M_{B,0}$ vs. time for the LATERS Markov model with the original volume averaged reaction rate $\langle r\rangle$ given by Eq. 18 and the volume averaged reaction rate equation without the fluctuation term from Eq. 24. These different equations of $\langle r\rangle$ tested the impact on the system when the fluctuation term is removed. Time is non-dimensionalized by a dispersion time scale defined as $\frac{\lambda^2}{D}$, where λ is the correlation length of the natural log of the permeability field and D is the constant dispersion coefficient

$\alpha\langle C'_A C'_B\rangle$, as well as the volume averaged reaction rate $\langle r\rangle$ versus time for the LATERS Markov model simulations with $\alpha = 1$, 1.1, 2, and 5. This Figure demonstrates that with increased magnitude of $\langle C'_A C'_B\rangle$ there is a decrease in the reaction rate $\langle r\rangle$ at early times before $\tilde{t} = 2\cdot 10^{-1}$. This decrease in $\langle r\rangle$ is particularly evident for $\alpha = 5$ and corresponds with the slowdown of reactions that was observed in Fig. 10a. With this decreased reaction rate, the system maintains more mass of the reactive solutes within the interface region, as expected. This, however, results in an increase of the mean term $\langle C_A\rangle\langle C_B\rangle$, which then causes $\langle r\rangle$ to rise as well. This explains the increase in reaction rate that was observed in Fig. 10d for the LATERS Markov model with $\alpha = 5$ around the time $\tilde{t} = 10^{-1}$. Eventually these mean and fluctuation terms reach a balance and we observe that the values of $\langle r\rangle$ are in good agreement at late times for all values of α considered in the upscaled model. This corresponds to the observation in Fig. 10a that all of the variations of the upscaled models are in agreement after $\tilde{t} \approx 4\cdot 10^{-1}$.

By implementing the LATERS Markov model with a modified volume averaged reaction rate equation given by Eq. 25, it is found that the magnitude of the fluctuation term $\langle C'_A C'_B\rangle$ is not the source of the over-prediction of reaction observed for $Da = 62.5$ in Sect. 5. In fact, even when $\alpha\langle C'_A C'_B\rangle$ is artificially increased, the slowdown in reactions caused by this term results in more reactant mass surviving at the interface. With more reactive solute mass in interface region, $\langle r\rangle$ increases and reactions begin to happen more quickly until these mean and fluctuation terms reach a balance.

6.2 How does grid resolution impact reaction rates?

In this section, we examine the role of grid resolution on the results of the upscaled model. The calculation of Eulerian reaction in the upscaled LATERS Markov model depends on two separate grids: one to calculate the concentration field and the other to calculate reaction. In Sect. 5, we showed results for the upscaled model with a concentration grid comprised of cells of size $l_{x,C} = l_{x,C} = \lambda = 2$ and a reaction grid with cells of size $l_{x,r} = l_{x,r} = L_{cell} = 48$. These grid resolutions based on the correlation length of the permeability field (λ) and the SMM cell length (L_{cell}) were selected because they correspond to physical length scales of the system. Here, we explore the impact of grid resolution on our upscaled reactive transport model by coarsening and refining the concentration and reaction grids.

First, we examine the impact of concentration grid resolution on the system. Figure 11 shows the total mass of the reactive solute B versus time for the LATERS Markov model with the original grid ($l_{x,C} = l_{x,C} = \lambda = 2$), a fine concentration grid resolution with $l_{x,C} = l_{x,C} = 1$, and a coarse concentration grid resolution of $l_{x,C} = l_{x,C} = 4\lambda = 8$. All three of these upscaled models have the same reaction grid resolution of $l_{x,r} = l_{x,r} = L_{cell} = 48$. From Fig. 11, it is clear that the concentration grid resolution has almost no impact on the results of the LATERS Markov model. In Sect. 6.1, it was observed that the fluctuation term $\langle C'_A C'_B\rangle$ in Eq. 18 has little effect on the upscaled system as a whole. Since the resolution of the concentration grid ultimately affects the calculation of this fluctuation term, it is unsurprising that the concentration grid resolution does not have a large impact on the results of the upscaled model.

Next, we examine the impact of the reaction grid resolution on the system. Fig. 12 shows the total mass of the reactive solute B in the system versus time for our original reaction grid resolution of $l_{x,r} = l_{x,r} = L_{cell} = 48$, a coarse grid resolution of $l_{x,r} = l_{x,r} = 2L_{cell} = 96$, and a fine grid resolution of $l_{x,r} = l_{x,r} = 4\lambda = 8$. The results of the upscaled model with a coarser grid resolution show a stronger over-prediction of reactions relative to the original grid. It is clear from Fig. 12 that the fine grid resolution case does a better job at the earlier times when the original and coarse grid cases were previously over-predicting

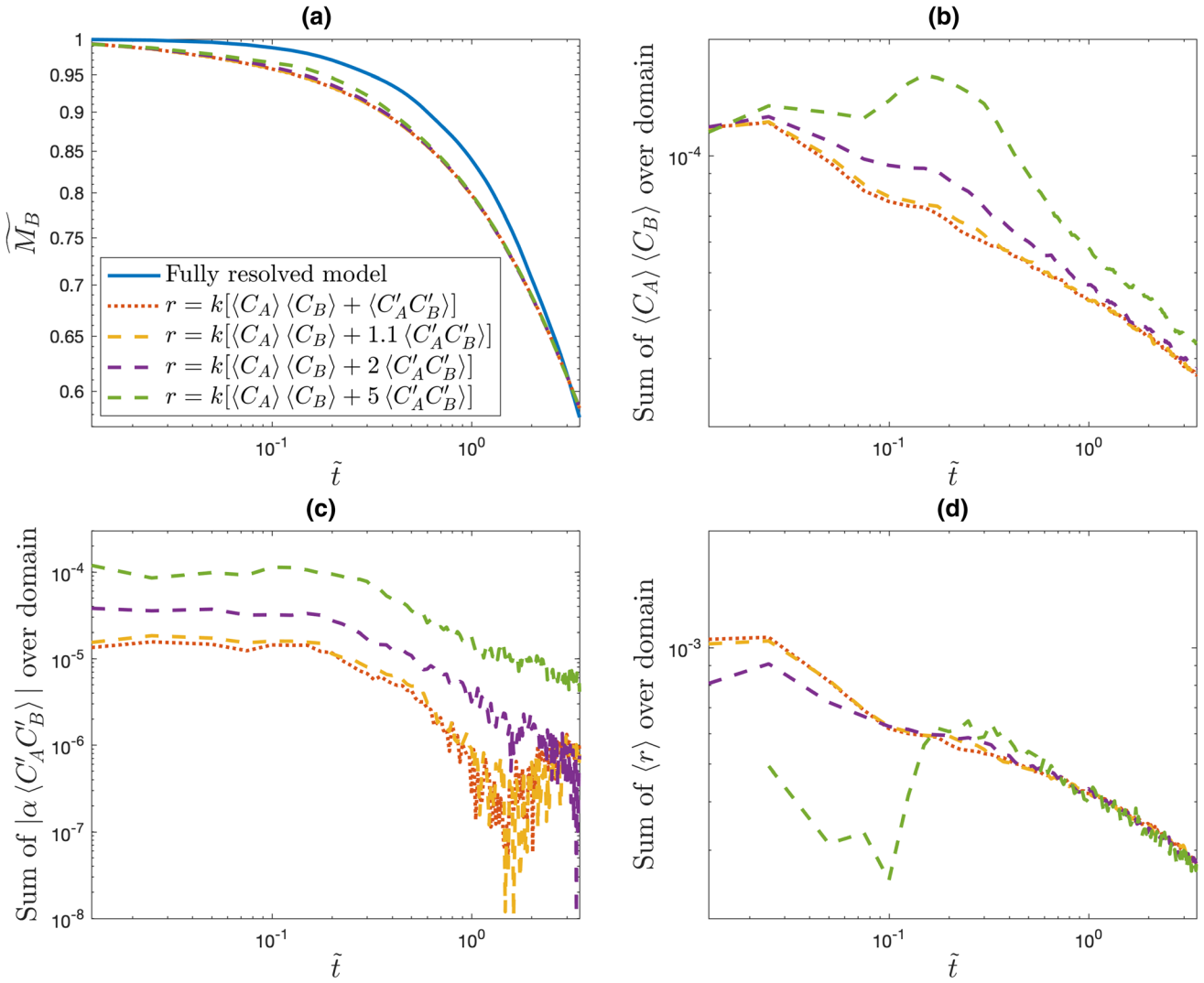

Fig. 10 (**a**) The total mass of B normalized by the total mass of B in the domain at time = 0, i.e. $\widetilde{M}_B = M_B/M_{B,0}$ and the sum of (**b**) $\langle C_A\rangle\langle C_B\rangle$, (c) the absolute value of $|\alpha\langle C'_A C'_B\rangle|$, and (d) $\langle r\rangle$ values over the whole domain versus time for the LATERS Markov model with four different versions of the volume averaged reaction rate $\langle r\rangle$ given by Eq. 25 with $\alpha = 1$, 1.1, 2, and 5. These modified $\langle r\rangle$ equations test the impact on the system when the fluctuation term has an artificially larger magnitude. Time is non-dimensionalized by a dispersion time scale defined as $\frac{\lambda^2}{D}$, where λ is the correlation length of the natural log of the permeability field and D is the constant dispersion coefficient

reactions. This is because the fine grid resolution is better able to capture the features of the incomplete mixing between the reactive solutes A and B that the fluctuation term $\langle C'_A C'_B\rangle$ in Eq. 18 is meant to account for in the LATERS Markov model framework. Figure 13 shows the volume averaged concentrations in the reaction grid cells averaged across the y-direction versus x at three different points in time throughout the simulation for the LATERS Markov model with the fine reaction grid resolution and the fully resolved model. By comparing Figs 13 and 7, it is clear that the fine reaction grid resolution does a much better job of predicting the amount of reaction in the interface between the reactive solutes A and B than with the original reaction grid.

It should also be noted that the upscaled model results appear to underpredict reactions at later times in Fig. 12. Since this feature appears to be most prominent for the fine grid resolution case, it is likely that this underprediction of reaction at late times occurs because reactions have depleted the solute particles within the size of the reaction volume. Reaction can only occur when both A and B particles exist within the same reaction grid cell, so the depletion of particles over this grid cell area will limit reactions that can occur on the Eulerian grid. Fine grid resolutions will be affected by this more quickly than coarser grid resolutions, and this discretization-based error aligns with the observed underprediction of reaction at late times in Fig. 12.

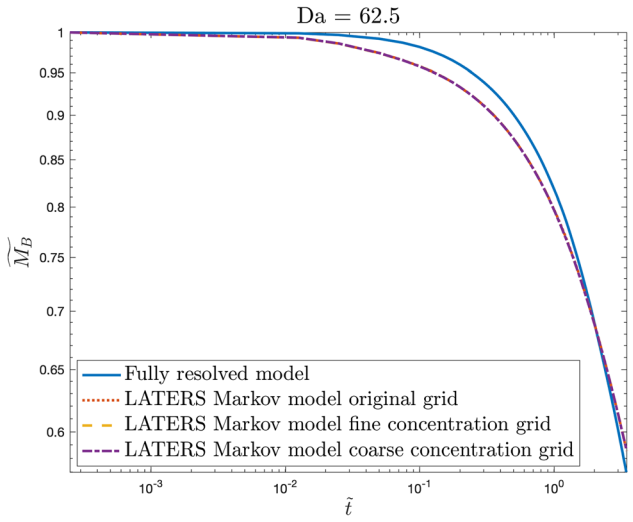

Fig. 11 The total mass of B in the domain normalized by the total mass of B in the domain at time = 0, i.e. $\widetilde{M_B} = M_B/M_{B,0}$ vs. time for $Da = 62.5$ with three different concentration grid resolutions that all have the same reaction grid resolution of $l_{x,r} = l_{x,r} = L_{cell} = 48$. First, the original case with a concentration grid resolution of $l_{x,C} = l_{x,C} = \lambda = 2$, the results of which were previously shown and discussed in Sect. 5. Second, a new fine grid case that has a concentration grid resolution of $l_{x,C} = l_{x,C} = 1$. Finally, a coarse grid case with a concentration grid resolution of $l_{x,C} = l_{x,C} = 4\lambda = 8$

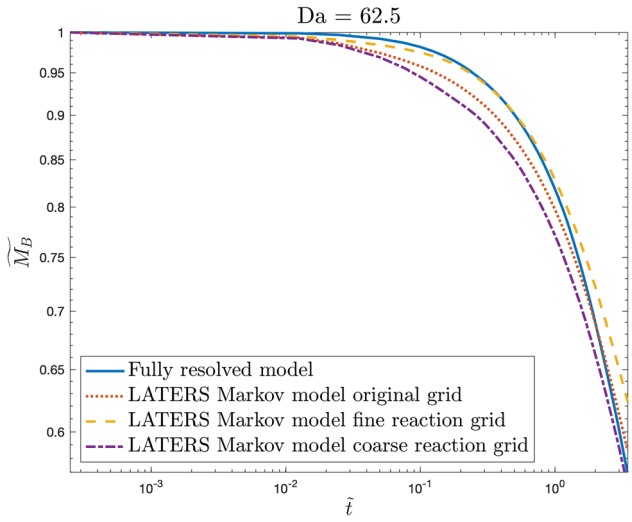

Fig. 12 The total mass of B in the domain normalized by the total mass of B in the domain at time = 0, i.e. $\widetilde{M_B} = M_B/M_{B,0}$ vs. time for $Da = 62.5$ with three different reaction grid resolutions. First, we have the original case with a concentration grid resolution of $l_{x,C} = l_{x,C} = \lambda = 2$ and a reaction grid resolution of $l_{x,r} = l_{x,r} = L_{cell} = 48$. The results for this case were previously shown and discussed in Sect. 5. Second, we have a new fine grid case that has a reaction grid resolution of $l_{x,r} = l_{x,r} = 4\lambda = 8$. Finally, we have a coarse grid case with a reaction grid resolution of $l_{x,r} = l_{x,r} = 2L_{cell} = 96$. Time is non-dimensionalized by a dispersion time scale defined as $\frac{\lambda^2}{D}$, where λ is the correlation length of the natural log of the permeability field and D is the constant dispersion coefficient

While it is found that the fine reaction grid resolution is better able to capture the appropriate amount of reaction at the times when the original and coarse reaction grid resolutions overpredicted reactions, the purpose of this work is to upscale reactive transport in this system. By moving toward higher resolution grids, we are losing the computational benefits of the upscaled model. However, the fact that this method more accurately captures the effects of incomplete mixing under higher grid resolution implies that transport in this system is being upscaled properly. The overprediction of reaction by the LATERS Markov model for higher Damköhler numbers must be a result of how reactions are calculated, and this is not simply a matter of increasing the magnitude of the upscaled reaction term as shown in the previous section.

6.3 How should we account for reactions within the upscaled model?

The results of Sects. 6.1 and 6.2 demonstrate that the cause of the overprediction of reaction by the LATERS Markov model must be from the upscaled reaction calculation and not upscaled transport. Here, we examine how the reaction calculation is implemented in the Lagrangian framework and its effect on the system. The results shown in this work thus far have been from simulations where upscaled reactions are calculated using a random particle killing procedure. In this method, a probability of reaction is calculated based on $\langle r \rangle$ for each of the reactive solutes A and B within every reaction grid cell at each time step. Then, particles within each reaction grid cell are assigned a random number $\xi \sim U(0, 1)$ and are selected for reaction if ξ is less than the probability of reaction. This method therefore treats all particles within a reaction cell as equally likely for reaction. Since we are considering reactions of the form $A + B \rightarrow \emptyset$, if a particle reacts it is removed from the system.

In the original LATERS Markov model developed by Sund et al. (2017), upscaled reaction is implemented differently with a particle mass reducing method. To account for reaction at every time step in that work, Sund et al. (2017) first calculates the amount of mass to be removed from each reaction grid cell. Next, they determine the total mass of the reactive solute within the reaction grid cell, subtract the amount of mass that must be removed due to reaction, and then distribute the remaining mass evenly among the particles in the cell. A detailed description of this procedure can be found in Sund et al. (2017).

Figure 14 shows the total mass of the reactive solute B in the system versus time for the fully resolved model and the LATERS Markov model with reactions calculated using the random particle killing method and the mass reducing method. It is observed in this Figure that the mass

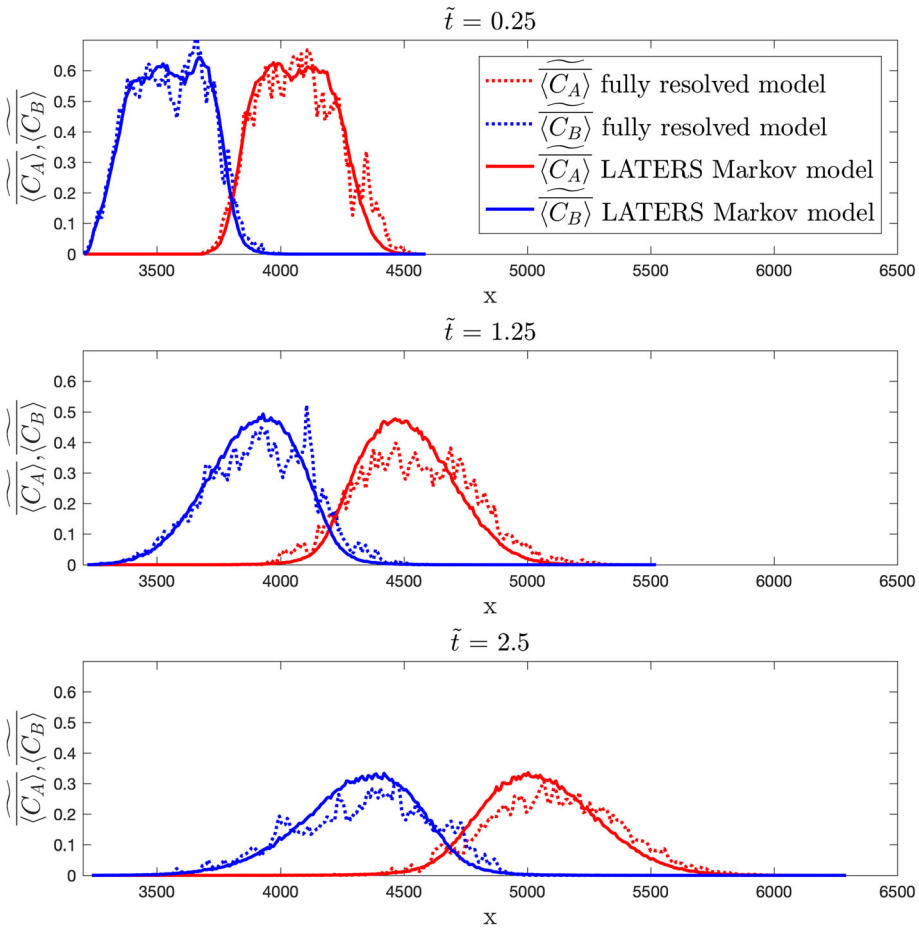

Fig. 13 $\widetilde{\langle C_A \rangle}$ and $\widetilde{\langle C_B \rangle}$ vs. x at times $\tilde{t} = 0.25$, 1.25, and 2.5 for $Da = 62.5$ for the fine grid case shown in Fig. 12. Here, the concentration grid has resolution $l_{x,C} = l_{x,C} = \lambda = 2$ and the reaction grid has resolution $l_{x,r} = l_{x,r} = 4\lambda = 8$. The overbar indicates an average over the reaction cells in the y direction and $\langle \bigstar \rangle$ indicates a volume average over a single reaction cell

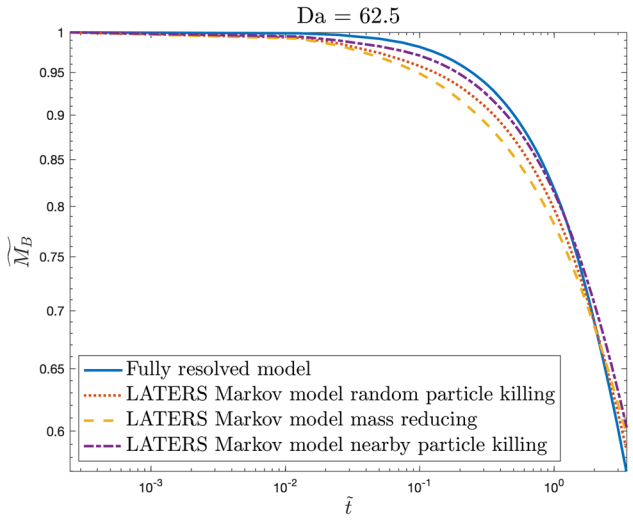

Fig. 14 The total mass of B in the domain normalized by the total mass of B in the domain at time = 0, i.e. $\widetilde{M}_B = M_B/M_{B,0}$ vs. time for the fully resolved model and the LATERS Markov model with (i) the particle killing method that has been used throughout this paper where particles are selected for reaction randomly within the reaction cell, (ii) the mass reducing method of Sund et al. (2017), and (iii) a particle killing method where nearby A and B particles within the reaction cell are selected for reaction

reducing method more strongly overpredicts the amount of reaction in the system than the random particle killing method. By distributing the remaining mass of the reactive solute evenly among the particles within each grid cell after reaction, the mass reducing method is causing an increase in mixing. This increased mixing of the solute mass results in more reactions, which is inconsistent with the highly local reactions expected at high *Da*.

It is demonstrated in Fig. 14 that the method by which reactions are executed has an effect on the system. In our random particle killing method, particles are selected for reaction randomly based on the probability of reaction in the cell. In reality, the particles that should be the most likely candidates for reaction are the A and B particles that are nearest to each other. To test the impact of this, we run the LATERS Markov model with a particle killing method that preferentially removes nearby A and B particles. With this reaction method, we first do a range search and determine which AB particle pairs are closest to each other in the reaction cell. Then, the probability of reaction is calculated as usual using Eq. 23, the number of particles to be removed for reaction is determined, and the closest AB pairs are removed for reaction. Figure 14 shows that the

Table 1 The mean absolute error of $\log_{10}(M_B)$ for each of the LATERS Markov model reaction methods as defined by Eq. 26 averaged over the specified times

Reaction Method	ϵ ($\tilde{t} = 0$ **to** 0.25)	ϵ ($\tilde{t} = 0$ **to** 1.25)	ϵ ($\tilde{t} = 0$ **to** 2.5)	ϵ ($\tilde{t} = 0$ **to** 3.5)
Random particle killing	0.0090	0.0114	0.0077	0.0080
Mass reducing	0.0133	0.0193	0.0131	0.0133
Nearby particle killing	0.0042	0.0036	0.0060	0.0102

nearby particle killing method does a much better job at accounting for incomplete mixing compared to the random particle killing method except at very late times. Table 1 shows the mean absolute error of $\widetilde{M_B}$ for each of the LATERS Markov model reaction methods as compared to the fully resolved model, defined by

$$\epsilon = \frac{\sum_{i=1}^{N_{pts}} |\log_{10}(\widetilde{M}_{B\,FullyResolved}) - \log_{10}(\widetilde{M}_{B\,LATERS})|}{N_{pts}}. \tag{26}$$

As shown in Table 1, the nearby particle killing method significantly reduces the error at all early and intermediate times up to approximately $\tilde{t} = 2.5$. At late times when the reactants have depleted in the interface, the random particle killing method performs the best. While adding a particle range search to the upscaled model does add some computational cost, it is limited because it only requires searches within reaction cells and not globally. Overall, these results indicate that this is an essential element that is needed for the LATERS Markov model to better predict effective reactive transport under high Damköhler conditions.

7 Conclusions

We extend the LATERS Markov model (Sund et al. 2017) to a more general non-uniform flow through an idealized heterogeneous porous medium. It is found that the upscaled model is able to predict effective reactive transport for reactions of the form $A + B \rightarrow \emptyset$ very well for systems with $Da = 0.625$ and $Da = 6.25$. While this method is able to upscale reactive transport for systems with lower Damköhler numbers, it did not do as well for high Da systems where incomplete mixing is expected to have a larger impact on the system. These results are consistent with the findings of Battiato et al. (2009), Battiato and Tartakovsky (2011), who concluded that reaction-dominated systems (i.e. high Da) are not favorable for upscaling. To identify the cause of the overprediction of reactions by the LATERS Markov model in high Da systems, we investigate the impact of the fluctuation term $\langle C'_A C'_B \rangle$ in the volume averaged reaction rate equation $\langle r \rangle$, the resolution of the concentration and reaction grids, and the method of removing solute mass for reaction on the upscaled model.

It is found that the upscaled term $\langle C'_A C'_B \rangle$ has very little impact on the results of the LATERS Markov model. Simulations where the estimated $\langle C'_A C'_B \rangle$ term is completely eliminated or manually increased in magnitude are examined, and the results are not significantly affected in either case.

After testing the LATERS Markov model on a variety of concentration and reaction grid resolutions, it is found that the reaction grid resolution has a significant impact on the results of the upscaled model. With a fine reaction grid resolution, we are able to better predict the amount of reaction in the system than the coarser grid resolutions that strongly overpredicted reactions. Since the upscaled model with a fine grid reaction grid resolution is able to capture the effects of incomplete mixing, this suggests that the model is successfully upscaling transport. This supports the results of Wright et al. (2019) where the downscaling procedures to select particle locations within the upscaled Spatial Markov model were able to predict the effective mixing of conservative transport within an acceptable margin of error. The cause of the overprediction of reaction in high Da systems must then be due to how reactions are calculated within the upscaled model.

To further investigate this point, we examine more closely the random particle killing method which involves calculating a probability of reaction within each reaction volume based on the value of $\langle r \rangle$. Particles within the reaction volume are then assigned a uniform random number $\xi \sim U(0, 1)$, and removed if the probability of reaction is greater than ξ. In the original LATERS Markov model developed by Sund et al. (2017), the authors accounted for reaction by calculating the total mass of the reactive solute within the reaction volume, removing the amount of mass designated for reaction, and then distributing the remaining mass evenly among all of the particles in the reaction volume. After implementing this method in our framework, it is found that the overprediction of reaction is significantly stronger than it is for the random particle killing method, since the method of Sund

et al. (2017) causes increased mixing by uniformly distributing the mass among the particles in the cell; this results in too much reaction over time because it falsely assumes that particles can equally likely react with all particles in the cell. Furthermore, the fact that these two methods of mass removal yield such different results demonstrates that the method by which mass is removed during the reaction step is very important.

The two random particle killing methods described above do not account for the fact that A and B particles that are near each other should be more likely to react with one another than those farther apart. We therefore test a nearby particle killing method where AB particle pairs that are closest to each other within the reaction cell are selected for reaction. This method does a much better job at correctly predicting the amount of reaction in the system than the random particle killing method. While adding a particle range search to the reaction step does add some computational expense, the upscaled model was still more than 10 times faster than the fully resolved model. These results demonstrate that it is crucial to account for the fact that nearby particles are more likely to react in order to better predict effective reactive transport in higher *Da* systems.

We conclude that upscaled reactive transport models require more information on smaller scales in systems where incomplete mixing is important. Local mixing effects that are critical for correct predictions of chemical reactions in such systems must be incorporated in the upscaled reaction calculations. In the LATERS Markov model, the transport and reaction processes are treated separately. It was determined that even when transport was accounted for properly, the method by which reactions are implemented will have a significant impact on the outcome of the system. In order to capture the effects of incomplete mixing in these higher *Da* systems, A and B particles that are near each other should be more likely to be selected for reaction than those that are farther apart in the upscaled model.

Our results open future pathways for the development and implementation of the proposed methods to quantify uncertainty related to reactive transport in heterogeneous media, e.g., within multi-realization ensembles where upscaling approaches can be used to considerably reduce the computational costs. In this framework, our analysis provides an evaluation of the approximation errors that can be expected as a function of the Da number.

Acknowledgements This work was supported by the US Army Research Office under contract/grant number W911NF-18-1-0338. The MATLAB scripts for the Fully Resolved and LATERS models can be found at https://github.com/RichterLab/LATERS-Markov-model.git.

References

Aarnes JE, Gimse T, Lie KA (2007) An introduction to the numerics of flow in porous media using matlab. Geometric modelling, numerical simulation, and optimization. Springer, Berlin, pp 265–306

Alhashmi Z, Blunt MJ, Bijeljic B (2015) Predictions of dynamic changes in reaction rates as a consequence of incomplete mixing using pore scale reactive transport modeling on images of porous media. J Contam Hydrol 179:171–181

Battiato I, Tartakovsky DM (2011) Applicability regimes for macroscopic models of reactive transport in porous media. J Contam Hydrol 120–121:18–26

Battiato I, Tartakovsky DM, Tartakovsky AM, Scheibe T (2009) On breakdown of macroscopic models of mixing-controlled heterogeneous reactions in porous media. Adv Water Resour 32(11):1664–1673

Benson DA, Aquino T, Bolster D, Engdahl N, Henri CV, Fernàndez-Garcia D (2017) A comparison of Eulerian and Lagrangian transport and non-linear reaction algorithms. Adv Water Resour 99:15–37

Benson DA, Meerschaert MM (2008) Simulation of chemical reaction via particle tracking: Diffusion-limited versus thermodynamic rate-limited regimes. Water Resources Research, 44

Benson DA, Pankavich S, Bolster D (2019) On the separate treatment of mixing and spreading by the reactive-particle-tracking algorithm: An example of accurate upscaling of reactive poiseuille flow. Adv Water Resour 123:40–53

Boso F, Bellin A, Dumbser M (2013) Numerical simulations of solute transport in highly heterogeneous formations: A comparison of alternative numerical schemes. Adv Water Resour 52:178–189

Chiogna G, Bellin A (2013) Analytical solution for reactive solute transport considering incomplete mixing within a reference elementary volume. Water Resour Res 49(5):2589–2600

Committee on Future Options for Management in the Nation's Subsurface Remediation Effort, Water Science and Technology Board, Division on Earth and Life Studies, and National Research Council. Alternatives for managing the nation's complex contaminated groundwater sites. National Academies Press, (2013)

de Anna P, Le Borgne T, Dentz M, Tartakovsky AM, Bolster D, Davy P (2013) Flow intermittency, dispersion, and correlated continuous time random walks in porous media. Phys Rev Lett 110(18):1–5

Dentz M, Le Borgne T, Englert A, Bijeljic B (2011) Mixing, spreading and reaction in heterogeneous media: A brief review. J Contam Hydrol 120–121:1–17

Ding D, Benson DA, Paster A, Bolster D (2013) Modeling bimolecular reactions and transport in porous media via particle tracking. Adv Water Resour 53:56–65

Edery Y, Scher H, Berkowitz B (2009) Modeling bimolecular reactions and transport in porous media. Geophys Res Lett 36:L02407

Edery Y, Scher H, Berkowitz B (2010) Particle tracking model of bimolecular reactive transport in porous media. Water Resour Res 46(7):1–12

Gillespie DT (2007) Stochastic simulation of chemical kinetics. Annu Rev Phys Chem 58(February):35–55

Ginn TR (2018) Modeling bimolecular reactive transport with mixing-limitation: Theory and application to column experiments. Water Resour Res 54(1):256–270

Gramling C, Harvey C, Meigs L (2002) Reactive transport in porous media: A comparison of model prediction with laboratory visualization. Environ Sci Technol 36(11):2508–2514

Kang K, Redner S (1984) Scaling approach for the kinetics of recombination processes. Phys Rev Lett 52(12):955–958

Kang PK, Anna P, Nunes JP, Bijeljic B, Blunt MJ, Juanes R (2014) Pore-scale intermittent velocity structure underpinning anomalous transport through 3-d porous media. Geophys Res Lett 41(17):6184–6190

Kang PK, Le Borgne T, Dentz M, Bour O, Juanes R (2015) Impact of velocity correlation and distribution on transport in fractured media: Field evidence and theoretical model. Water Resources Research 51(2):940–959

Kang PK, Brown S, Juanes R (2016) Emergence of anomalous transport in stressed rough fractures. Earth Planet Sci Lett 454:46–54

Kang PK, Dentz M, Juanes R (2011) Predictability of anomalous transport on lattice networks with quenched disorder. Phys Rev E 83(3):030101

Kang PK, Dentz M, Le Borgne T, Juanes R (2011) Spatial Markov model of anomalous transport through random lattice networks. Phys Rev Lett 107(18):1–5

Kang PK, Dentz M, Le Borgne T, Juanes R (2015) Anomalous transport on regular fracture networks: Impact of conductivity heterogeneity and mixing at fracture intersections. Phys Rev E 92(2):022148

Kang PK, Dentz M, Le Borgne T, Lee S, Juanes R (2017) Anomalous transport in disordered fracture networks: Spatial Markov model for dispersion with variable injection modes. Adv Water Resour 106:80–94

Knutson C, Valocchi A, Werth C (2007) Comparison of continuum and pore-scale models of nutrient biodegradation under transverse mixing conditions. Adv Water Resour 30(6–7):1421–1431

Le Borgne T, Bolster D, Dentz M, De Anna P, Tartakovsky A (2011) Effective pore-scale dispersion upscaling with a correlated continuous time random walk approach. Water Resour Res 47(12):1–10

Le Borgne T, Dentz M, Carrera J (2008) Lagrangian statistical model for transport in highly heterogeneous velocity fields. Phys Rev Lett 101(9):1–4

Le Borgne T, Dentz M, Carrera J (2008) Spatial Markov processes for modeling Lagrangian particle dynamics in heterogeneous porous media. Phys Rev E - Stat, Nonlinear, Soft Matter Phys 78(2):1–9

Mayer KU, Benner SG, Blowes DW (2006) Process-based reactive transport modeling of a permeable reactive barrier for the treatment of mine drainage. J Contam Hydrol 85(3–4):195–211

Monson E, Kopelman R (2000) Observation of laser speckle effects and nonclassical kinetics in an elementary chemical reaction. Phys Rev Lett 85(3):666–669

Monson E, Kopelman R (2004) Nonclassical kinetics of an elementary A+B->C reaction-diffusion system showing effects of a speckled initial reactant distribution and eventual self-segregation: Experiments. Phys Rev E - Stat, Nonlinear, Soft Matter Phys 69(21):1–12

Ovchinnikov AA, Zeldovich YB (1978) Role of density fluctuations in bimolecular reaction kinetics. Chem Phys 28(1–2):215–218

Paster A, Aquino T, Bolster D (2015) Incomplete mixing and reactions in laminar shear flow. Phys Rev E 92(1):012922

Paster A, Bolster D, Benson DA (2013) Particle tracking and the diffusion-reaction equation. Water Resour Res 49(1):1–6

Paster A, Bolster D, Benson David A (2014) Connecting the dots: Semi-analytical and random walk numerical solutions of the diffusionreaction equation with stochastic initial conditions. J Comput Phys 263:91–112

Porta GM, Riva M, Guadagnini A (2012) Upscaling solute transport in porous media in the presence of an irreversible bimolecular reaction. Adv Water Resour 35:151–162

Porta GM, Ceriotti G, Thovert J-F (2016) Comparative assessment of continuum-scale models of bimolecular reactive transport in porous media under pre-asymptotic conditions. J Contam Hydrol 185:1–13

Rolle M, Chiogna G, Hochstetler DL, Kitanidis PK (2013) On the importance of diffusion and compound-specific mixing for groundwater transport: An investigation from pore to field scale. J Contam Hydrol 153:51–68

Sanchez-Vila X, Fernàndez-Garcia D, Guadagnini A (2010) Interpretation of column experiments of transport of solutes undergoing an irreversible bimolecular reaction using a continuum approximation. Water Resour Res 46(12):1–7

Steefel CI, DePaolo DJ, Lichtner PC (2005) Reactive transport modeling: An essential tool and a new research approach for the Earth sciences. Earth Planet Sci Lett 240(3–4):539–558

Sund N, Porta G, Bolster D, Parashar R (2017) A Lagrangian transport Eulerian reaction spatial (LATERS) Markov model for prediction of effective bimolecular reactive transport. Water Res Res 53(11):9040–58

Toussaint D, Wilczek F (1983) Particle antiparticle annihilation in diffusive motion. J Chem Phys 78(5):2642

Wright EE, Richter DH, Bolster D (2017) Effects of incomplete mixing on reactive transport in flows through heterogeneous porous media. Phys Rev Fluids 2(11):114501

Wright EE, Sund NL, Richter DH, Porta GM, Bolster D (2019) Upscaling mixing in highly heterogeneous porous media via a spatial markov model. Water 11:53

Yeh GT, Tripathi VS (1989) A critical evaluation of recent developments in hydrogeochemical transport models of reactive multichemical components. Water Resour Res 25(1):93–108